HHS Public Access

Author manuscript

Magn Reson Imaging. Author manuscript; available in PMC 2018 February 01.

Published in final edited form as:

Magn Reson Imaging. 2017 February ; 36: 121–127. doi:10.1016/j.mri.2016.10.026.

Dependence on b-Value of the Direction-Averaged Diffusion-Weighted Imaging Signal in Brain

Emilie T. McKinnon[a,b,c], **Jens H. Jensen**[b,c,*], **G. Russell Glenn**[b,c,d], and **Joseph A. Helpern**[a,b,c,d]

[a] Department of Neurology, Medical University of South Carolina, Charleston, South Carolina, USA

[b] Center for Biomedical Imaging, Medical University of South Carolina, Charleston, South Carolina, USA

[c] Department of Radiology and Radiological Science, Medical University of South Carolina, Charleston, South Carolina, USA

[d] Department of Neuroscience, Medical University of South Carolina, Charleston, South Carolina, USA

Abstract

Purpose—The dependence of the direction-averaged diffusion-weighted imaging (DWI) signal in brain was studied as a function of b-value in order to help elucidate the relationship between diffusion weighting and brain microstructure.

Methods—High angular resolution diffusion imaging (HARDI) data were acquired from two human volunteers with 128 diffusion-encoding directions and six b-value shells ranging from 1000 to 6000 s/mm^2 in increments of 1000 s/mm^2. The direction-averaged signal was calculated for each shell by averaging over all diffusion-encoding directions, and the signal was plotted as a function of b-value for selected regions of interest. As a supplementary analysis, we also applied similar methods to retrospective DWI data obtained from the human connectome project (HCP), which includes b-values up to 10,000 s/mm^2.

Results—For all regions of interest, a simple power law relationship accurately described the observed dependence of the direction-averaged signal as a function of the diffusion weighting. In white matter, the characteristic exponent was 0.56 ± 0.05, while in gray matter it was 0.88 ± 0.11. Similar results were obtained with the HCP data.

Conclusion—The direction-averaged DWI signal varies, to a good approximation, as a power of the b-value, for b-values between 1000 and 6000 s/mm^2. The exponents characterizing this power law behavior were markedly different for white and gray matter, indicative of sharply contrasting

*Corresponding author: Jens H. Jensen, Center for Biomedical Imaging, Department of Radiology and Radiological Science, Medical University of South Carolina, 96 Jonathon Lucas St., MSC 323, Charleston, SC 29425-0323, jense@musc.edu, Telephone: 843-876-2467.

microstructural environments. These results may inform the construction of microstructural models used to interpret the DWI signal.

Keywords

HARDI; b-value; diffusion; brain; microstructure; MRI

1. Introduction

The relationship between the diffusion-weighted imaging (DWI) signal and brain tissue microstructure is subtle and manifold. In white matter, there is the added complexity of substantial diffusion anisotropy caused by axonal fiber bundles. While there have been a variety of mathematical models proposed to describe this relationship, their relative merits are still debated, and this topic continues to be actively investigated [1,2].

Previously proposed models include bi-exponentials [3-7], stretched exponentials [8] and power laws [9,10]. Although each of these approaches can approximately fit DWI data over significant ranges of b-values, their precise mathematical forms are quite different, as is particularly evident for large b-values. For bi-exponential models, the large b-value behavior will be dominated by the more slowly decreasing term, and so it will approach a simple mono-exponential decay. For stretched exponentials, the signal decay has the form $\exp[-(kb)^a]$, where b is the b-value, k is a constant, and $a < 1$ parameterizes the degree of stretching. For the statistical model of Yablonskiy and coworkers [9], the signal decays as $1/b$ for large b, while for the model considered by Jensen and coworkers [10] , the large b signal decays as $1/\sqrt{b}$.

In order to investigate the b-value dependence of the DWI signal, we acquired high angular resolution diffusion imaging (HARDI) data from two healthy volunteers with b-values ranging from 1000 to 6000 s/mm^2 in increments of 1000 s/mm^2 and with 128 uniformly distributed diffusion-encoding directions for each b-value shell. We then averaged the signal for each shell over all of the diffusion-encoding directions in order to reduce the effects of variable degrees of diffusion anisotropy [11]. In effect, this corresponds to determining the powder-averaged signal [12], which should have a less complicated behavior than the full signal. Related data reduction methods have been applied to DWI in various contexts [7,11,13]. Here our purpose is to suppress the effects of macroscopic diffusion anisotropy, as quantified by metrics such as the fractional anisotropy (FA). Nonetheless, the direction-averaged DWI signal will still reflect microscopic diffusion anisotropy, as is often studied with double diffusion encoding MRI [14-16] and magic-angle spinning DWI [17]. As a supplementary analysis, we also applied similar methods to retrospective DWI data obtained from the human connectome project (HCP), which includes b-values up to 10,000 s/mm^2 [18].

Remarkably, our results demonstrate a simple power law scaling of the direction-averaged DWI signal throughout the brain parenchyma over the range of b-values considered. Moreover, a distinct qualitative difference is found between white and gray matter, suggesting sharp biophysical differences beyond just macroscopic diffusion anisotropy. We

discuss the significance of our observations with respect to the mathematical modeling of the DWI signal. However, our main purpose here is not to compare how well different models fit our data, but rather to describe the empirical dependence on the b-value of the direction-averaged DWI signal and the broader implications of this for modeling.

2. Material and methods

2.1 Data acquisition

Data were acquired from two healthy volunteers (Subject 1, female, age 25 yr; Subject 2, male, age 55 yr) under a protocol approved by our institutional review board using a Siemens 3T TIM Trio MRI scanner (Siemens Healthcare, Erlangen, Germany) and a 32 channel head coil (adaptive combine mode). HARDI data were acquired for six b-value shells using a twice-refocused DWI sequence in order to reduce eddy current distortion [19]. The b-values for the shells were 1000, 2000, 3000, 4000, 5000 and 6000 s/mm^2, and each shell had the same 128 uniformly distributed diffusion-encoding directions over half a sphere, determined with an electrostatic repulsion algorithm [20]. Fourteen images without diffusion weighting (b0 images) were acquired at the beginning of each session, and one additional b0 image was acquired between each b-value shell. Other acquisition parameters were TE = 149 ms, TR = 7200 ms, slice thickness = 3.0 mm, field of view = 222×222 mm^2, pixel bandwidth = 1351 Hz/px, echo spacing = 0.82 ms, and parallel imaging factor = 2. The acquisition matrix was 74×74 resulting in an in-plane resolution of 3×3 mm^2 with a total scan time of 97 min 31 s.

For anatomical reference, magnetization-prepared rapid gradient echo (MPRAGE) images were acquired with 192 sagittal slices, TE = 2.3 ms, TR = 1900 ms, TI = 900 ms and slice thickness = 1 mm. The field of view was 256×256 mm^2, yielding 1 mm^3 isotropic voxels. The total scan time for the MPRAGE acquisition was 4 min and 26 s.

2.2 Image analysis

Due to the lengthy scan time, a co-registration process was implemented to account for motion, using Statistical Parametric Mapping (SPM8, Wellcome Department of Imaging Neuroscience, London, United Kingdom). The images for each b-value shell were co-registered with a rigid body transformation to the average of the initial set of fourteen b0 images, employing each shell's respective intermediate b0 image as the source image. The MPRAGE images were also brought into diffusion space by using the average of all b0 images as a template. To reduce the contribution of signal noise and Gibbs ringing [21], all diffusion-weighted images were smoothed with a Gaussian kernel having a full width at half maximum of 3.75 mm [22].

The direction-averaged diffusion-weighted images were calculated with the following image analysis steps. In order to estimate the average over all gradient directions, one million random points were selected on the surface of a sphere with unit radius and with the origin at the sphere's center. For each point, we determined the closest gradient vector by calculating the angle between that point and each of the 128 gradient vectors. Subsequently, a weight was assigned to each gradient vector by the fraction of assigned closest points over

the sphere. This fraction was then applied to calculate a weighted average of all the diffusion-weighted images for each shell. This weighted average is more accurate than an unweighted average, since even “uniformly distributed” points typically do not have exactly equal spacings [23].

The regions of interest (ROIs) were defined by the following semi-automated method. First subcortical segmentations were obtained by using the raw MPRAGE images together with FreeSurfer v5.0 (Freesurfer, Laboratory for Computational Neuroimaging, Charlestown, MA). Details on the FreeSurfer subcortical segmentations are described by Fischl et al. [24]. Next, the segmentations were brought into diffusion space by employing the same affine transformation matrix used to transform the MPRAGE image. Additionally, certain white matter regions, such as the splenium and the cerebellar peduncle, were obtained from the John Hopkins University (JHU) white matter atlas [25]. Finally, the segmentations of FreeSurfer, the JHU white matter labels, and the MPRAGE images were yoked together, and four voxels in the core of each selected anatomical region were defined manually. These small ROIs were chosen to increase the likelihood that they contained a single tissue type without partial volume contamination, possibly introduced by the long acquisition time, low spatial resolution and smoothing. The following anatomical regions were analyzed: cerebellar peduncle, splenium, internal capsule, frontal white matter, thalamus, cerebellar gray matter, and putamen (Fig. 1). For the purposes of this study, we classified the ROIs drawn for internal capsule, splenium, frontal white matter and cerebellar peduncle as being white matter brain tissue. Conversely, regions selected from thalamus, cerebellar gray matter and putamen were regarded as being gray matter (although the thalamus does contain some white matter). The SNR was estimated in each ROI from the ratio of the average signal for the 6000 s/mm^2 b-value shell to the average background signal (for a similar number of voxels) multiplied by $(\pi/2)^{1/2}$ [26,27]. All statistical tests performed under Results are paired t-tests, with a significance level of p = 0.05, not corrected for multiple comparisons.

The direction-averaged DWI signal for each b-value shell was normalized by dividing by the b0 signal on a voxel-by-voxel basis. For both subjects, this normalized mean signal was further averaged over the selected ROIs, and the resulting data were graphed on a log-log plot. Linear fits to these data were then determined by linear regression, with the slope, intercept and their associated errors determined according to standard methods [28]. We also calculated the quantity

$$\zeta = 2 \cdot \sqrt{\frac{b}{\pi}} \cdot \frac{\bar{S}}{S_0} , \quad (1)$$

where b is the b-value, $\bar{S}$ is the direction-averaged DWI signal, and S_0 is the signal for $b = 0$. Recent work has argued that

$$\zeta \approx \frac{f}{\sqrt{D_a}} , \quad (2)$$

for white matter if the b-value is sufficiently large, where f is the fraction of MRI visible water inside axons and D_a is the intrinsic intra-axonal diffusivity (i.e., the along-axis diffusivity of water inside axons) [10].

2.3 Supplementary Analysis

In order to test the generalizability of our results, we also performed a retrospective analysis for one subject (female, age between 25-29) from the MGH Adult Diffusion Dataset downloaded from the HCP data repository (https://www.humanconnectome.org). This dataset was acquired on a 3T Siemens Connectom scanner, customized with a 64 channel tight-fitting brain array coil [29] and consists of MPRAGE and diffusion scans with four levels of diffusion weighting. The b-values used were 1000, 3000, 5000 and 10,000 s/mm^2 with respectively 64, 64, 128 and 256 randomly distributed diffusion-encoding directions over a full sphere. Every 14th volume was an image without diffusion weighting (b0) used for motion correction. Other acquisition parameters were TE = 57 ms, TR = 8800 ms, voxel size = 1.5 mm^3 isotropic, field of view = 210×210 mm^2, pixel bandwidth = 1984 Hz/Px, echo spacing = 0.63 ms and parallel imaging factor = 3. Additional details can be found in [30]. The MPRAGE acquisition parameters were TE = 1.15 ms, TR = 2530 ms, TI = 1100 ms, and voxel size = 1 mm^3 isotropic voxels.

These data were analyzed in a manner very similar to that described above for our primary dataset with a few notable differences. First, the Gaussian smoothing kernel had a full width at half maximum of 1.85 mm, due to the higher resolution of the HCP data. Second, we computed the direction-averaged signal for each b-value shell from a simple arithmetic mean. Since the HCP diffusion encoding directions are random, this arithmetic mean corresponds to a conventional Monte Carlo integration divided by the number of directions [31]. Finally, because of the higher resolution of the HCP dataset, each ROI consisted of 16 rather than 4 voxels.

3. Results

For Subject 1, the SNR at b = 6000 s/mm^2 ranged from 6.3 to 11.4 in the white matter ROIs and between 3.1 and 6.6 in the gray matter ROIs. For Subject 2, the ranges were 8.5-11.2 for white matter and 3.0-4.9 for gray matter. This suggests that the bias in our data due to rectified noise should be relatively small [26].

The log-log plotted ROI data for Subject 1 together with linear fits are shown in Fig. 2a. The x-axis corresponds to $\ln(b_1/b)$, while the y-axis corresponds $\ln\left(\bar{S}/S_0\right)$. Here $b_1 \equiv 1000$ s/mm^2 is a reference b-value scale, chosen for convenience. The high quality of these linear fits (average R^2 of 0.996) indicates that, over the range of b-values investigated, the data are well described by power law behavior of the form

$$\frac{\bar{S}}{S_0} \approx C \left(\frac{b_1}{b}\right)^{\alpha}, \quad (3)$$

where the exponent α is the measured slope of the fits and C is a dimensionless constant. The constant C is approximately equal to $\bar{S}_{1000}/S_0$, with $\bar{S}_{1000}$ being the direction-averaged signal for $b \equiv 1000$ s/mm^2, and may be calculated directly from the y-intercept of the fits.

The fact that the direction-averaged DWI signal is accurately fit by a power law for b = 1000 to 6000 s/mm^2 indicates that two degrees of freedom are sufficient to describes the b-value dependence over this range of diffusion weightings. This is further illustrated in Fig. 2b by linear scale power law fits of $\bar{S}$ as a function of the b-value. The quality of these fits is remarkable given that they utilize only two adjustable parameters. In contrast, a stretched exponential [8] has three adjustable parameters, while a bi-exponential [7] uses four.

Following Eq. (3), we computed for each ROI both the exponent α and the constant C, which were derived from the slope and y-intercept of the linear regression analysis of the log data (as in Fig. 2a). Table 1 lists these fitting parameters for both subjects and all the ROIs. In white matter, the mean exponent α is found to be 0.56 ± 0.05, while the mean gray matter exponent has a substantially larger value of 0.88 ± 0.11. A paired t-test demonstrates the white and gray matter exponents to be significantly different (p = 0.0005). The fitting constant is, C in contrast, relatively similar over the considered ROIs, with no significant difference between its average values calculated from white matter (0.53 ± 0.03) and gray (0.48 ± 0.05).

Parametric maps of α for a single axial slice from each subject are shown in Fig. 3. Corresponding FA maps [32] and MPRAGE images are also provided for anatomical reference. The FA maps were calculated from a conventional diffusional kurtosis imaging analysis using just the images with diffusion weightings of b = 0, 1000 and 2000 s/mm^2 [22]. Throughout the white matter, the exponent is seen to be relatively close to 0.5, while appreciably larger values are found for gray matter in consistency with our ROI results. Voxels containing substantial amounts of cerebrospinal fluid (e.g., ventricles and sulci) also show large values of α in Fig. 3, but this may be of little physical significance as the signal in these regions does not necessarily follow the power law decay of Eq. (3).

By combining Eqs. (1) and (2), one finds

$$\frac{\bar{S}}{S_0} \approx \frac{\zeta}{2}\sqrt{\frac{\pi}{b}} \quad . \qquad (4)$$

This has the same form as Eq. (3) with an exponent $\alpha = 0.5$, which is relatively close to the measured values for white matter shown in Table 1. Thus our observed power law decay is roughly consistent with the behavior predicted by Eq. (4). Parametric maps of ζ, as derived with Eq. (1), from one subject for each of the b-values considered in this experiment are shown in Fig. 4. Within the white matter regions, the ζ estimates for the higher b-values are seen to be relatively consistent with each other, as would be expected for a true tissue property. Bar graphs of the ζ estimates for the white matter ROIs based on the b = 4000 s/mm^2 HARDI data are given by Fig. 5a. The mean values over all of the white matter ROIs are shown as a function of the b-value in Fig. 5b, again indicating a stable behavior for the

larger diffusion weightings. The fact that ζ is a decreasing function for the lower b-values, suggests that including this lower range of b-values in the calculation of the power law exponent α tends to increase its value.

For the HCP dataset, the SNR at b=10,000 s/mm^2 is 3.9-5.4 in white matter ROIs and 3.0-4.9 in gray matter ROIs. For gray matter this is comparable to the SNR of our primary dataset, but the white matter SNR is somewhat lower. The linear regression ROI fits are shown in Fig. 6a. For all the white matter regions and for the cerebellar gray matter ROI, the data points from all four b-values lie close to the best fit lines, indicating approximate power law decay. The R^2 values for the white matter regions ranges from 0.995 to 0.999, cerebellar gray matter has $R^2 = 0.997$. The R^2 values for the thalamus and putamen are 0.955 and 0.965, which is somewhat lower than we find with our primary dataset. This may indicate a breakdown of power law scaling, but could also reflect a systematic error in the measurements. The deviation from linearity in these two gray matter regions is most pronounced in the $b = 10{,}000$ s/mm^2 data points, which also correspond to the two data points with the lowest SNR. Although our simple SNR estimates are suggestive of minor noise bias, this is not definitive given the complex nature of noise when parallel imaging is utilized [33]. In this regard, it is important to note that the HCP data was acquired with a parallel imaging factor of 3, while the primary dataset used a parallel imaging factor of 2. The exponents obtained from the best fit lines in Fig. 6a had an average value of $\alpha = 0.48 \pm 0.05$ for white matter and $\alpha = 0.73 \pm 0.13$ for gray matter, which is fairly similar to, if a bit lower than, the values from our primary dataset. The region-by-region comparison of the HCP exponents with those for the primary dataset is given by Fig 6b. A parametric map of α for one slice of the HCP data appears in Fig. 6c, along with FA and MPRAGE images. Overall, in most white matter regions, the values for α are a little above 0.5, but they are visibly lower in high FA areas such as the corpus callosum.

4. Discussion

The central observation of this paper is the simple power law behavior of the direction-averaged DWI signal, as given by Eq. (3), for b-values ranging from 1000 to 6000 s/mm^2. In white matter, the average measured exponent is $\alpha = 0.56 \pm 0.05$, while the average gray matter exponent of 0.89 ± 0.11 is substantially larger. This disparity suggests fundamental differences in gray and white matter microstructure. Due to the direction averaging of the DWI signal, we hypothesize that these go beyond those reflected in the familiar macroscopic diffusion anisotropy metrics (e.g., FA) [32].

It should be emphasized that our primary data only support power law signal decay for the restricted range of b-values between 1000 and 6000 s/mm^2. For smaller b-values, this scaling behavior must break down as the DWI signal approaches a constant in the limit $b \rightarrow 0$. It could also fail to hold for very large b-values, if, for example, there were a pool of immobile proton spins that contributed a constant to the overall signal. However, our supplementary analysis of HCP data suggests that this picture may indeed hold for b-values as high 10,000 s/mm^2, although the acquisition parameters for the HCP dataset are quite different from ours. Most importantly, the TE for our dataset is 149 ms, while HCP dataset was acquired with TE = 57 ms. This implies a much shorter diffusion time as well as a larger

contribution from myelin water for the HCP dataset, which could potentially affect the quality of the power law decay fits. In addition, the HCP dataset includes only 64 diffusion encoding directions for b = 1000 s/mm^2 and 3000 s/mm^2, which would reduce the accuracy of the directional averaging, especially in high FA areas such as the corpus callosum.

The exponent of approximately one-half for white matter is consistent with the large b-value limit predicted for a model of water confined to thin, impermeable cylindrical tubes [10,34], which is commonly used to describe the diffusion dynamics of intra-axonal water [34-37]. Our results support this as being a reasonable approximation for white matter (Table 1, Fig. 3). However, the markedly larger exponent found for gray matter points to essential differences in the diffusion dynamics. Since gray matter does contain a large proportion of neurites that are plausibly modeled by thin cylindrical tubes [34-37], this conclusion may seem surprising. Indeed by using magnetic resonance spectroscopy, Kroenke and coworkers [35] measured the diffusion-weighted signal decay for N-acetyl-L-aspartate (NAA) in rat brain up to b-values of about 20,000 s/mm^2 and showed that this data could be accurately fit with a model based on thin, impermeable cylinders. The volume elements for the experiment were large, but contained substantial amounts of gray matter. Thus, the higher exponent found here for water diffusion most likely reflects a distinction between water and NAA diffusion dynamics, rather than simply the geometry of the cylinder model being inadequate for gray matter. One key distinction is that NAA is confined to neurons [35], while water can cross cell membranes. The discrepancy between the white and gray matter exponents for our experiment could then plausibly be due to gray/white matter differences in water permeability for the cell membranes of neurites, with gray matter having a sufficiently larger permeability to invalidate the model. Thus, qualitatively different assumptions about brain microstructure may be necessary to accurately model the water diffusion dynamics for white and gray matter.

As discussed by Jensen and coworkers [10], a consequence of the thin cylindrical tube model for axons is that the direction-averaged DWI signal decay in white matter can be related to the microstructural parameter ζ, in the limit of large b-values. Estimates for ζ obtained from our data and Eq. (1) are shown in Figs. 4 and 5. These estimates are fairly consistent across b-values for b ≥ 4000 s/mm^2. As intrinsic tissue parameters must be independent of the diffusion weighting, this suggests a reasonable minimum b-value of about 4000 s/mm^2 for the applicability of Eq. (4). Since the estimations of both the intra-axonal diffusivity, D_a, and the axonal water fraction f are topics of substantial recent interest [38], accurate quantification of $\zeta \equiv f/\sqrt{D_a}$ from data acquired from a single b-value shell could be useful in constraining microstructural models of water diffusion dynamics in brain [1,39]. As is evident from Figs. 4 and 5, there is some variability in ζ values across white matter regions. From our results alone, it cannot be determined whether this is mainly due to differences in f or D_a. However, individual estimates for these parameters based on explicit modeling suggest that both of these parameters may have significant regional variations [37,39,40].

Two other proposed models predict power law signal decay, at least for sufficiently large b-values. One of these is the statistical model of Yablonskiy and coworkers [9], for which the signal decays as $1/b$ for large b. This does not match the power law behavior that we find in

white matter, but it is in rough agreement with our exponent for gray matter. Yet another statistical model, based on a gamma distribution of diffusion coefficients, yields a DWI signal of the form [41-43].

$$\frac{S}{S_0} = \frac{1}{(1+b/b_c)^{\epsilon}} , \quad (5)$$

which scales as $(b_c/b)^{\varepsilon}$ for $b \gg b_c$. However, in this case, the exponent ε depends on the details of the distribution rather than having a universal value. Nonetheless, it should be emphasized once again that our observation of power law scaling for the direction-averaged DWI signal has only been demonstrated over a restricted range of b-values, and so our results may not be sufficient to fully evaluate either of these two statistical models.

Note added in revision: While this paper was under review, an independent study reported similar power law scaling for the direction-averaged DWI signal in white matter with an exponent near one-half up to b-values of 10,000 s/mm^2 [44].

5. Conclusions

The direction-averaged DWI signal in human brain decreases with increasing b-values approximately as a power law, for b-values ranging from 1000 to 6000 s/mm^2. In white matter, the exponent characterizing this decrease is close to one-half, which is consistent with the large b-value limit of a model in which intra-axonal water diffusion is confined to thin, impermeable cylinders. The exponent for gray matter is substantially larger, indicative of sharp microstructural differences relative to white matter that likely go beyond those associated with diffusion anisotropy. As a consequence, in contrast to some previous approaches, white and gray matter may require distinct tissue modeling strategies in order to obtain the most accurate results.

6. Acknowledgements

This work was supported in part by the National Institutes of Health grant T32GM008716 (to P. Halushka) and by the Litwin Foundation (to J.A.H).

Abbreviations

DWI	diffusion-weighted imaging
HARDI	high angular resolution diffusion imaging
MPRAGE	magnetization-prepared rapid gradient echo
ROI	region of interest
FA	fractional anisotropy
HCP	Human Connectome Project
NAA	N-acetyl-L-aspartate

7. References

[1]. Panagiotaki E, Schneider T, Siow B, Hall MG, Lythgoe MF, Alexander DC. Compartment models of the diffusion MR signal in brain white matter: a taxonomy and comparison. Neuroimage. 2012; 59(3):2241–54. [PubMed: 22001791]

[2]. Mulkern RV, Haker SJ, Maier SE. On high b diffusion imaging in the human brain: ruminations and experimental insights. Magn Reson Imaging. 2009; 27(8):1151–62. [PubMed: 19520535]

[3]. Niendorf T, Dijkhuizen RM, Norris DG, van Lookeren Campagne M, Nicolay K. Biexponential diffusion attenuation in various states of brain tissue: implications for diffusion-weighted imaging. Magn Reson Med. 1996; 36(6):847–57. [PubMed: 8946350]

[4]. Clark CA, Le Bihan D. Water diffusion compartmentation and anisotropy at high b values in the human brain. Magn Reson Med. 2000; 44(6):852–9. [PubMed: 11108621]

[5]. Clark CA, Hedehus M, Moseley ME. In vivo mapping of the fast and slow diffusion tensors in human brain. Magn Reson Med. 2002; 47(4):623–8. [PubMed: 11948721]

[6]. Mulkern RV, Gudbjartsson H, Westin CF, Zengingonul HP, Gartner W, Guttmann CR, Robertson RL, Kyriakos W, Schwartz R, Holtzman D. Multi-component apparent diffusion coefficients in human brain. NMR Biomed. 1999; 12(1):51–62. others. [PubMed: 10195330]

[7]. Maier SE, Mulkern RV. Biexponential analysis of diffusion-related signal decay in normal human cortical and deep gray matter. Magn Reson Imaging. 2008; 26(7):897–904. [PubMed: 18467062]

[8]. Bennett KM, Schmainda KM, Bennett RT, Rowe DB, Lu H, Hyde JS. Characterization of continuously distributed cortical water diffusion rates with a stretched-exponential model. Magn Reson Med. 2003; 50(4):727–34. [PubMed: 14523958]

[9]. Yablonskiy DA, Bretthorst GL, Ackerman JJ. Statistical model for diffusion attenuated MR signal. Magn Reson Med. 2003; 50(4):664–9. [PubMed: 14523949]

[10]. Jensen JH, Russell Glenn G, Helpern JA. Fiber ball imaging. Neuroimage. 2015; 124:824–833. Pt A. [PubMed: 26432187]

[11]. Kaden E, Kruggel F, Alexander DC. Quantitative mapping of the per-axon diffusion coefficients in brain white matter. Magn Reson Med. 2016; 75(4):1752–63. [PubMed: 25974332]

[12]. Eden M. Computer simulations in solid-state NMR. III. Powder averaging. Concepts in Magnetic Resonance Part A. 2003; 18A(1):24–55.

[13]. Basser PJ, Pierpaoli C. A simplified method to measure the diffusion tensor from seven MR images. Magn Reson Med. 1998; 39(6):928–34. [PubMed: 9621916]

[14]. Shemesh N, Jespersen SN, Alexander DC, Cohen Y, Drobnjak I, Dyrby TB, Finsterbusch J, Koch MA, Kuder T, Laun F. Conventions and nomenclature for double diffusion encoding NMR and MRI. Magn Reson Med. 2016; 75(1):82–7. others. [PubMed: 26418050]

[15]. Jespersen SN, Lundell H, Sonderby CK, Dyrby TB. Orientationally invariant metrics of apparent compartment eccentricity from double pulsed field gradient diffusion experiments. NMR Biomed. 2013; 26(12):1647–62. [PubMed: 24038641]

[16]. Hui ES, Jensen JH. Double-pulsed diffusional kurtosis imaging for the in vivo assessment of human brain microstructure. Neuroimage. 2015; 120:371–81. [PubMed: 26172309]

[17]. Lasic S, Szczepankiewicz F, Eriksson S, Nilsson M, Topgaard D. Microanisotropy imaging: quantification of microscopic diffusion anisotropy and orientational order parameter by diffusion MRI with magic-angle spinning of the q-vector. Frontiers in Physics. 2014; 2:11.

[18]. McNab JA, Edlow BL, Witzel T, Huang SY, Bhat H, Heberlein K, Feiweier T, Liu K, Keil B, Cohen-Adad J. The Human Connectome Project and beyond: initial applications of 300 mT/m gradients. Neuroimage. 2013; 80:234–45. others. [PubMed: 23711537]

[19]. Reese TGH, Weisskoff RM, Wedeen VJ. Reduction of eddy-current-induced distortion in diffusion MRI using a twice-refocused spin echo. Magn Reson Med. 2003; 49(1):177–82. O. [PubMed: 12509835]

[20]. Jones DK, Horsfield MA, Simmons A. Optimal strategies for measuring diffusion in anisotropic systems by magnetic resonance imaging. Magn Reson Med. 1999; 42(3):515–25. [PubMed: 10467296]

[21]. Veraart, J., Fieremans, E., Jelescu, IO., Knoll, F., Novikov, DS. Gibbs ringing in diffusion MRI. Magn Reson Med. 2015. http://dx.doi.org/10.1002/mrm.25866

[22]. Tabesh A, Jensen JH, Ardekani BA, Helpern JA. Estimation of tensors and tensor-derived measures in diffusional kurtosis imaging. Magn Reson Med. 2011; 65(3):823–36. [PubMed: 21337412]

[23]. Saff EB, Kuijlaars AB. Distributing many points on a sphere. Math intelligencer. 1997; 19(1):5–11.

[24]. Fischl B, Salat DH, Busa E, Albert M, Dieterich M, Haselgrove C, van der Kouwe A, Killiany R, Kennedy D, Klaveness S. Whole brain segmentation: automated labeling of neuroanatomical structures in the human brain. Neuron. 2002; 33(3):341–55. others. [PubMed: 11832223]

[25]. Mori, S., Wakana, S., van Zijl, PCM. MRI atlas of human white matter. Elsevier; Amsterdam: 2005. Nagae-Poetscher LM; p. 284

[26]. Henkelman RM. Measurement of signal intensities in the presence of noise in MR images. Med Phys. 1985; 12(2):232–3. [PubMed: 4000083]

[27]. Gudbjartsson H, Patz S. The Rician distribution of noisy MRI data. Magn Reson Med. 1995; 34(6):910–4. [PubMed: 8598820]

[28]. Young, HD. Statistical Treatment of Experimental Data. McGraw-Hill; New York: 1962.

[29]. Keil B, Blau JN, Biber S, Hoecht P, Tountcheva V, Setsompop K, Triantafyllou C, Wald LL. A 64-channel 3T array coil for accelerated brain MRI. Magn Reson Med. 2013; 70(1):248–58. [PubMed: 22851312]

[30]. Setsompop K, Kimmlingen R, Eberlein E, Witzel T, Cohen-Adad J, McNab JA, Keil B, Tisdall MD, Hoecht P, Dietz P. Pushing the limits of in vivo diffusion MRI for the Human Connectome Project. Neuroimage. 2013; 80:220–33. others. [PubMed: 23707579]

[31]. Press, WH., Teukolsky, SA., Flannery, BP. Numerical Recipes in C: The Art of Scientifc Computing. Cambridge University Press; New York: 1992. p. 305W.T. V

[32]. Pierpaoli C, Basser PJ. Toward a quantitative assessment of diffusion anisotropy. Magn Reson Med. 1996; 36(6):893–906. [PubMed: 8946355]

[33]. Dietrich O, Raya JG, Reeder SB, Reiser MF, Schoenberg SO. Measurement of signal-to-noise ratios in MR images: influence of multichannel coils, parallel imaging, and reconstruction filters. J Magn Reson Imaging. 2007; 26(2):375–85. [PubMed: 17622966]

[34]. Yablonskiy DA, Sukstanskii AL. Theoretical models of the diffusion weighted MR signal. NMR Biomed. 2010; 23(7):661–81. [PubMed: 20886562]

[35]. Kroenke CD, Ackerman JJ, Yablonskiy DA. On the nature of the NAA diffusion attenuated MR signal in the central nervous system. Magn Reson Med. 2004; 52(5):1052–9. [PubMed: 15508157]

[36]. Jespersen SN, Kroenke CD, Ostergaard L, Ackerman JJ, Yablonskiy DA. Modeling dendrite density from magnetic resonance diffusion measurements. Neuroimage. 2007; 34(4):1473–86. [PubMed: 17188901]

[37]. Zhang H, Schneider T, Wheeler-Kingshott CA, Alexander DC. NODDI: practical in vivo neurite orientation dispersion and density imaging of the human brain. Neuroimage. 2012; 61(4):1000–16. [PubMed: 22484410]

[38]. Jelescu IO, Veraart J, Fieremans E, Novikov DS. Degeneracy in model parameter estimation for multi-compartmental diffusion in neuronal tissue. NMR Biomed. 2016; 29(1):33–47. [PubMed: 26615981]

[39]. Hui ES, Russell Glenn G, Helpern JA, Jensen JH. Kurtosis analysis of neural diffusion organization. Neuroimage. 2015; 106:391–403. [PubMed: 25463453]

[40]. Fieremans E, Jensen JH, Helpern JA. White matter characterization with diffusional kurtosis imaging. Neuroimage. 2011; 58(1):177–88. [PubMed: 21699989]

[41]. Jensen JH, Helpern JA. MRI quantification of non-Gaussian water diffusion by kurtosis analysis. NMR Biomed. 2010; 23(7):698–710. [PubMed: 20632416]

[42]. Roding M, Bernin D, Jonasson J, Sarkka A, Topgaard D, Rudemo M, Nyden M. The gamma distribution model for pulsed-field gradient NMR studies of molecular-weight distributions of polymers. J Magn Reson. 2012; 222:105–11. [PubMed: 22864268]

[43]. Szczepankiewicz F, Lasic S, van Westen D, Sundgren PC, Englund E, Westin CF, Stahlberg F, Latt J, Topgaard D, Nilsson M. Quantification of microscopic diffusion anisotropy disentangles effects of orientation dispersion from microstructure: applications in healthy volunteers and in brain tumors. Neuroimage. 2015; 104:241–52. [PubMed: 25284306]

[44]. Veraart J, Fieremans E, Novikov DS. Universal power-law scaling of water diffusion in human brain defines what we see with MRI. arXiv preprint; arXiv:1609.09145 [physics.bio-ph].

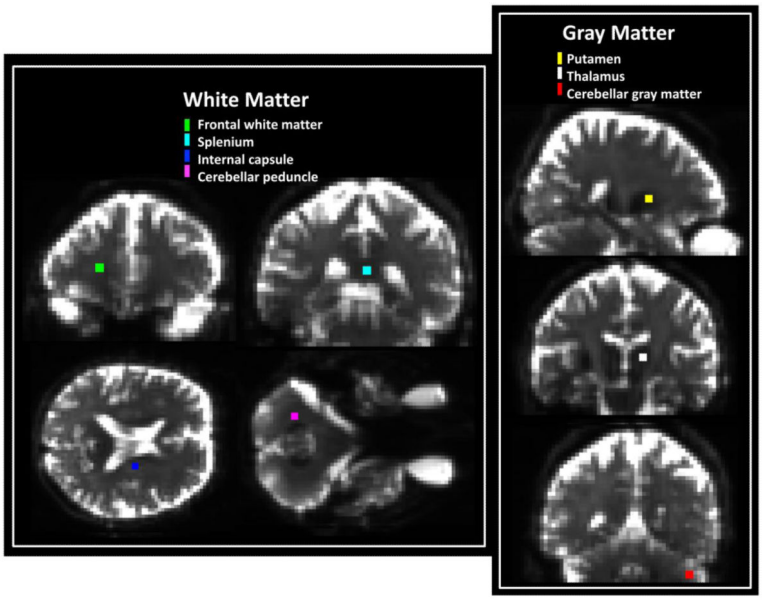

Figure 1.

Locations of the seven ROIs considered in the quantitative analysis superimposed on the average b0 image for one subject. Each ROI represents the core of a different anatomical region. Cerebellar peduncle (violet), splenium (cyan), internal capsule (blue) and frontal white matter (green) are all regarded as white matter regions, for the purposes of this study, while cerebellar gray matter (red), putamen (yellow) and thalamus (white) are classified as gray matter.

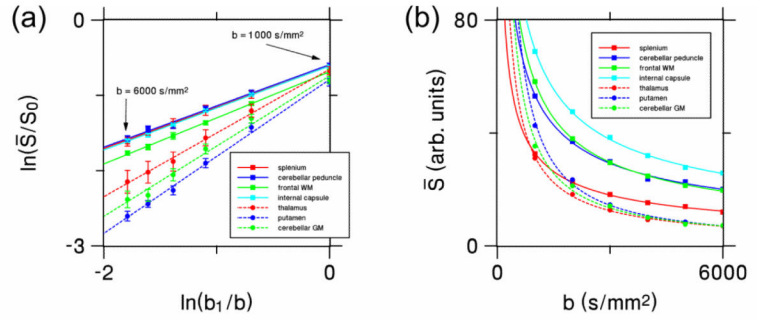

Figure 2.

(a) Log-log plot showing the relationship between the direction-averaged DWI signal $\bar{S}$ from each ROI (normalized by dividing by the signal without diffusion weighting, S_0) and the six b-values (1000, 2000, 3000, 4000, 5000 and 6000 s/mm^2) for all the ROIs of Subject 1. The reference b-value b_1 is set to 1000 s/mm^2. The error bars show the standard deviations of the measurements. The fits to Eq. (1) for white and gray matter regions are indicated by solid and dashed lines, respectively. (b) Linear scale plot showing the same data, but without normalization and error bars in order to better demonstrate the quality of the fits. WM = white matter; GM = gray matter.

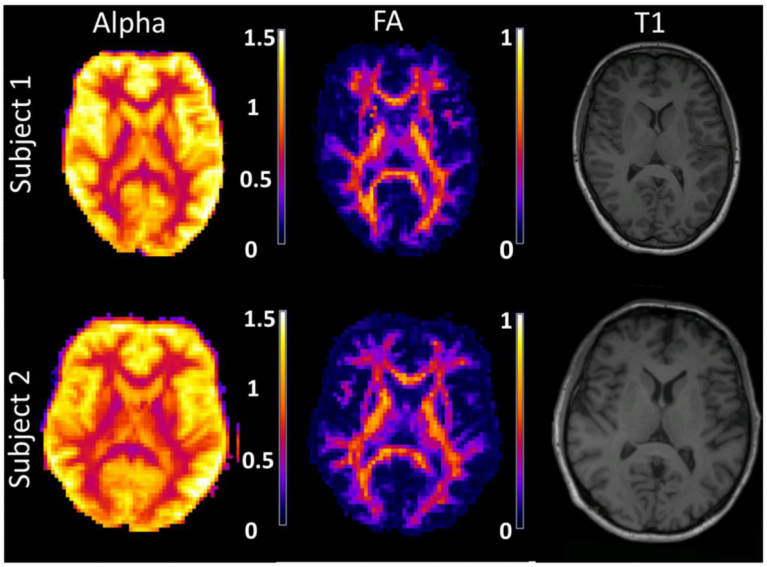

Figure 3.

Parametric maps of the exponent α for a single axial slice from each subject. For reference, the corresponding FA and a similar MPRAGE (T1) images are also shown. In white matter, α is close to 0.5, while for gray matter regions the exponent is consistently larger.

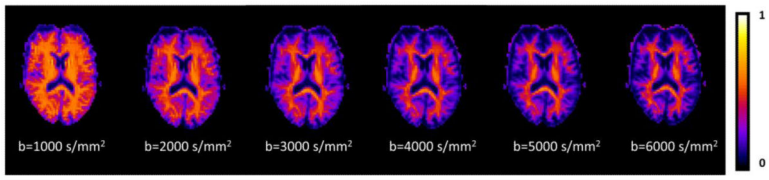

Figure 4.

Axial maps of estimates for the quantity ζ, as given by Eq. (1), for a single human subject as a function of the b-value. From the theory of Ref. 10, the estimates in white matter are expected to converge, for large b-values, to a level that is characteristic of the tissue microstructure. The scale bar is in units of $ms^{1/2}/\mu m$.

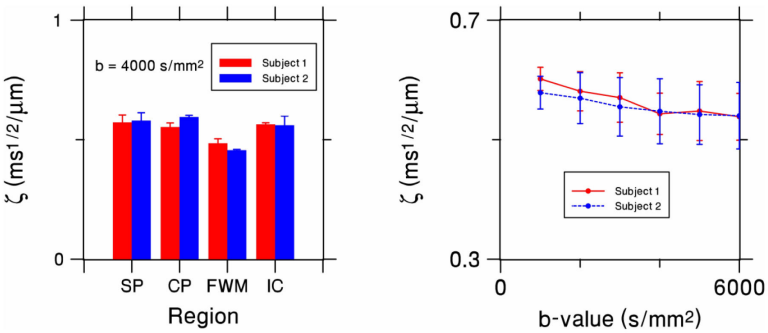

Figure 5.

(a) The quantity ζ for the four white matter ROIs as estimated with Eq. (1) and the HARDI data for b = 4000 s/mm^2. (b) Mean ζ values for all the white matter ROIs as a function of the b-value. The mean values for b = 4000, 5000, and 6000 s/mm^2 are all similar, in consistency with the theory of Ref. 10. All error bars indicate standard deviations. SP = splenium; CP = cerebellar peduncle; FWM = frontal white matter; IC = internal capsule.

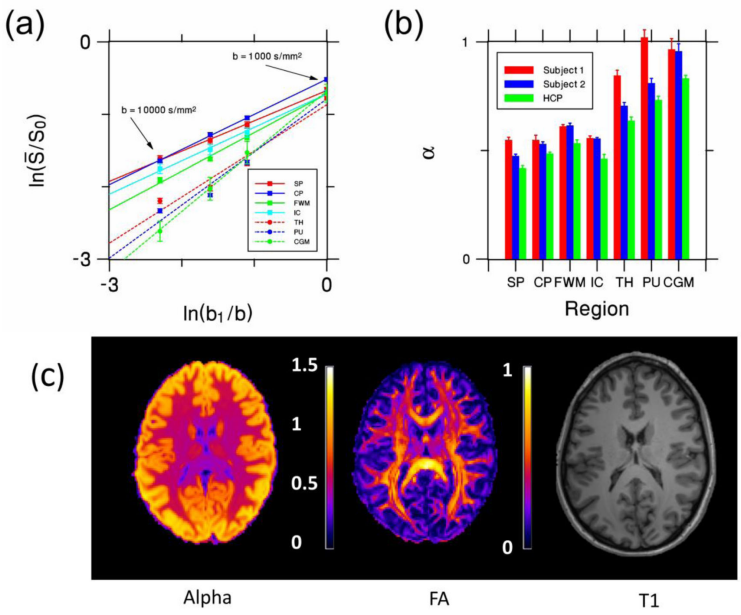

Figure 6.

(a) Log-log plot showing the relationship between the direction-averaged DWI signal $\bar{S}$ from each ROI (normalized by dividing by the signal without diffusion weighting, S_0) and the four b-values (1000, 3000, 5000, 10,000 s/mm^2) for all the ROIs in the HCP dataset (Similar to Fig 2a). (b) The exponent α for each ROI and subject. The HCP estimates are similar to those from the primary dataset. (c) Parametric maps of the exponent α and FA for a single axial slice from the HCP dataset. A similar T1 slice is provided as an anatomical reference. All error bars indicate standard deviations. SP = splenium; CP = cerebellar peduncle; FWM = frontal white matter; IC = internal capsule, TH = thalamus, PU = putamen, CGM = cerebellar gray matter.

Table 1

Estimates for the exponent α and scale constant C tained by fitting Eq. [3] to the direction-averaged DWI data from the six b-value shells for each of the subjects and the considered anatomical regions. The quality of the fits is indicated by the coefficient of determination R^2, and the uncertainties, in parentheses, indicate standard errors as determined with linear regression.

ROI		Subject 1			Subject 2		
		R^2	α	C	R^2	α	C
White Matter	cerebellar peduncle	0.993	0.548 (0.022)	0.553 (0.015)	0.999	0.530 (0.010)	0.545 (0.007)
	splenium	0.998	0.548 (0.013)	0.543 (0.008)	0.999	0.475 (0.008)	0.495 (0.005)
	internal capsule	0.998	0.557 (0.010)	0.543 (0.007)	0.999	0.555 (0.005)	0.537 (0.004)
	frontal	0.999	0.611 (0.008)	0.503 (0.008)	0.999	0.615 (0.011)	0.482 (0.006)
Gray Matter	thalamus	0.997	0.845 (0.024)	0.520 (0.016)	0.998	0.706 (0.015)	0.481 (0.009)
	cerebellum	0.989	0.966 (0.049)	0.485 (0.030)	0.995	0.957 (0.034)	0.397 (0.017)
	putamen	0.995	1.021 (0.034)	0.543 (0.020)	0.997	0.810 (0.022)	0.478 (0.013)